

ARTICLE OPEN



Cortical amyloid-beta burden is associated with changes in intracortical myelin in cognitively normal older adults

Marina Fernandez-Alvarez ^{1,2}, Mercedes Atienza^{1,2} and Jose L. Cantero ^{1,2}✉

© The Author(s) 2023

Amyloid-beta (A β) aggregates and myelin breakdown are among the earliest detrimental effects of Alzheimer's disease (AD), likely inducing abnormal patterns of neuronal communication within cortical networks. However, human in vivo evidence linking A β burden, intracortical myelin, and cortical synchronization is lacking in cognitively normal older individuals. Here, we addressed this question combining ¹⁸F-Florbetaben-PET imaging, cortical T1-weighted/T2-weighted (T1w/T2w) ratio maps, and resting-state functional connectivity (rs-FC) in cognitively unimpaired older adults. Results showed that global A β burden was both positively and negatively associated with the T1w/T2w ratio in different cortical territories. Affected cortical regions were further associated with abnormal patterns of rs-FC and with subclinical cognitive deficits. Finally, causal mediation analysis revealed that the negative impact of T1w/T2w ratio in left posterior cingulate cortex on processing speed was driven by A β burden. Collectively, these findings provide novel insights into the relationship between initial A β plaques and intracortical myelin before the onset of cognitive decline, which may contribute to monitor the efficacy of novel disease-modifying strategies in normal elderly individuals at risk for cognitive impairment.

Translational Psychiatry (2023)13:115; <https://doi.org/10.1038/s41398-023-02420-7>

INTRODUCTION

The accumulation and aggregation of amyloid-beta (A β) isoforms into senile plaques is the earliest recognizable event in Alzheimer's disease (AD). These first A β deposits precede overt clinical symptoms by decades [1–5] and they supposedly instigate the pathogenic cascade that leads to cognitive decline [6]. This hypothesis is supported by evidence indicating that subtle memory decline begins to appear with subthreshold amyloid PET [7]. Notably, early A β deposition initiates in weakly myelinated cortical regions [2], suggesting that A β plaques and abnormal cortical myelination are coupled events years before the onset of clinical manifestations.

Converging research has reinforced the link between cerebral A β pathology and myelin damage. In this context, in vitro experiments have shown that exposure to A β _{1–42} not only impairs the function of rodent oligodendrocytes and oligodendrocyte progenitor cells [8, 9] but also inhibits myelin sheet formation [10]. These findings have also been confirmed in transgenic mouse models that overexpress the amyloid precursor protein (APP) [11–14]. Evidence also supports the hypothesis that myelin breakdown drives A β pathology. Accordingly, myelin damage not only precedes A β deposition [15, 16] but also promotes plaque formation in mouse models of AD [17]. Regardless of whether myelin alterations precede or result from A β deposition, there is lack of evidence supporting associations between cortical A β burden and cortical myelin content in cognitively normal older people, which may contribute to monitor the efficacy of novel disease-modifying strategies on early A β toxicity in individuals at risk for cognitive decline.

Here, we investigated whether variations in global A β load parallel cortical changes in the T1-weighted/T2-weighted (T1w/T2w) ratio in cognitively unimpaired older adults. The T1w/T2w ratio is considered a measure of the microstructural integrity of the normal-appearing cortical grey matter (GM) [18] able to detect intracortical myelin content [19]. Based on evidence showing that early A β pathology initiates in poorly myelinated areas of the human neocortex [2], our prediction was that cortical A β burden, as revealed by ¹⁸F-Florbetaben-PET imaging, would be associated with lower T1w/T2w ratio in late-myelinating cortical regions.

Previous studies have revealed that subtle changes in myelination affect the speed of action potential conduction, thereby influencing neural circuit dynamic and precision in neuronal communication [20–23]. On the basis of this evidence, we hypothesized that cortical regions exhibiting correlations between T1w/T2w ratio and global A β load will also show impaired patterns of resting-state functional connectivity (rs-FC) and associations with subclinical cognitive deficits. Given that age-related slowing in cognitive processing speed seems to be mediated by myelin breakdown [24], we expected processing speed to be particularly associated with cortical regions affected by the relationship between T1w/T2w ratio and global A β burden, although other cognitive functions may also be similarly affected [25].

METHODS

Participants

Seventy-four cognitively normal older adults participated in the study (66.5 ± 5.7 years; range: 54–76 years; 51 females). They were recruited from

¹Laboratory of Functional Neuroscience, Pablo de Olavide University, Seville, Spain. ²CIBERNED, Network Center for Biomedical Research in Neurodegenerative Diseases, Madrid, Spain. ✉email: jicanlor@upo.es

Received: 20 December 2022 Revised: 24 March 2023 Accepted: 27 March 2023

Published online: 06 April 2023

Table 1. Demographic and cognitive profile of the study sample.

Age	66.5 ± 5.7
Sex (F/M)	51/23
Education years	12.5 ± 4.9
ApoE4 (yes/no)	16/58
MMSE	29.0 ± 1.2
Memory Binding Test	
Total free recall	15.5 ± 4.4
Total paired recall	24.6 ± 4.2
Total delayed-free recall	16.4 ± 4.9
Total delayed paired recall	24.0 ± 4.6
S-FNAME	32.6 ± 15.2
Boston Naming Test	12.1 ± 2.1
Phonological fluency	15.7 ± 4.4
Semantic fluency	22.0 ± 17.0
Trail Making Test-A	47.0 ± 21.5
Trail Making Test-B	119.5 ± 67.7
Tower of London	319.3 ± 113.2
D2	364.1 ± 94.0
Letter-number sequencing	9.1 ± 2.3
Digit span	14.3 ± 3.2
Symbol digit modalities test	38.5 ± 12.2

Results are expressed as mean ± standard deviation (SD), unless otherwise stated. F/M females/males; MMSE Mini Mental State Examination; S-FNAME Spanish validation of the Face Name Associative Memory Exam.

senior citizen's associations, health-screening programs, and hospital outpatient services. All of them underwent neurological and neuropsychological assessment to discard the presence of objective cognitive impairment and/or dementia. Individuals with medical conditions affecting brain structure or function (e.g., cerebrovascular disease, epilepsy, head trauma, history of neurodevelopmental disease, alcohol abuse, hydrocephalus, and/or intracranial mass) were not included in the study. Participants met the following criteria: i) normal global cognitive status in the Mini-Mental State Examination (scores ≥ 26); ii) normal cognitive performance in the neuropsychological tests relative to appropriate reference values for age and education level; iii) global score of 0 (no dementia) in the Clinical Dementia Rating; iv) functional independence as assessed by the Spanish version of the Interview for Deterioration in Daily Living Activities; [26] v) scores ≤ 5 (no depression) in the short form of the Geriatric Depression Scale; [27] and vi) not be taking medications that affected cognition, sleep, renal and/or hepatic function. All participants gave informed consent to the experimental protocol approved by the Ethical Committee for Clinical Research of the Junta de Andalucía according to the principles outlined in the Declaration of Helsinki. Table 1 contains sample characteristics.

Neuropsychological assessment

Subjects were administered with a neuropsychological battery to assess memory, attention, processing speed, and executive function skills such as working memory, inhibition, flexibility and planning. Neuropsychological tests included the Spanish version of the memory binding test (MBT) [28], the face-name associative memory exam (S-FNAME) [29], the D2 test, the letter-number sequencing and the digit span subtests of the Wechsler Adult Intelligence Scale-III, the spatial span subtest of the Wechsler Memory Scale-III, the short form of the Boston naming test (BNT), the semantic and phonological fluency tests based on the "Animal" and letter "P" naming tasks, the symbol digit modalities test, the two forms of the trail making test (TMT-A and TMT-B), and the tower of London (TL). All scores were z transformed. Inverse z-values were used in those cases where higher scores corresponded to worse performance. We further computed the Spearman's 'g' factor as an index of global cognitive function. This analysis was done with R Statistical Software v3.0.1 (R

Foundation for Statistical Computing, Vienna, Austria) using the *prcomp* function. We only retained the first component (eigenvalue 8.7), which explained 37.7% of variance in the data.

MRI acquisition, preprocessing, and generation of T1w/T2w ratio maps

Images were acquired on a 3 T Philips Ingenia MRI scanner using a 32-channel receive-only radio-frequency (RF) head coil and a transmit RF body coil (Philips, Best, Netherlands). The following MRI sequences were acquired in the same session: i) 3D T1-weighted (T1w) magnetization prepared rapid gradient echo (MPRAGE) in the sagittal plane: repetition time (TR)/echo time (TE) = 2600 ms/4.7 ms, flip angle (FA) = 9°, acquisition matrix = 384 × 384, voxel resolution in acquisition = 0.65 mm³ isotropic, resulting in 282 slices without gap between adjacent slices; ii) 3D T2w VISTA Turbo Spin Echo scan in the sagittal plane: TR/TE: 2500 ms/251 ms, FA = 90°, acquisition matrix = 384 × 384 mm, voxel resolution in acquisition = 0.65 mm³ isotropic, resulting in 282 slices without gap between adjacent slices; and iii) T2w Fast Field Echo images using a blood-oxygen-level-dependent (BOLD) sensitive single-shot echo-planar imaging (EPI) sequence in the axial plane: TR/TE: 2000 ms/30 ms, FA = 80°, acquisition matrix = 80 × 80 mm, voxel resolution in acquisition = 3 mm³ isotropic, resulting in 35 slices acquired in posterior to anterior phase-encoding direction with 1 mm of gap between adjacent slices. Pulse and respiratory rates were simultaneously recorded using the scanner's built-in pulse oximeter placed on the left-hand index finger and a pneumatic respiratory belt strapped around the upper abdomen, respectively. Before starting the acquisition of the EPI sequence, participants were asked to remain still and keep their eyes closed without falling sleep. We acquired 250 EPI scans preceded by 4 dummy volumes to allow time for equilibrium in the spin excitation. To allow for optimal B1 shimming, a B1 calibration scan was applied before starting the EPI sequence. Brain images were visually examined after each MRI sequence; they were repeated if artifacts were identified. All participants underwent the same protocol in the same MRI scanner at the research MRI facility located at Pablo de Olavide University.

T1w scans were preprocessed using Freesurfer v6.0 (<https://surfer.nmr.mgh.harvard.edu/>). The Freesurfer's pipeline included brain extraction, automated tissue segmentation, generation of white matter (WM) and pial surfaces, correction of surface topology and inflation, co-registration, and projection of cortical surfaces to a sphere for the purpose of establishing a surface-based coordinate system [30]. Pial surface misplacements and erroneous WM segmentation were manually corrected on a slice-by-slice basis by one experienced technician. T2w images were registered to T1w images with *bbregister* using a trilinear interpolation method and a boundary-based cost function constrained to 6 degrees of freedom [31].

Individual T1w/T2w ratio volumes were sampled at the halfway between the WM and GM surface, resulting in midthickness surface maps of the T1w/T2w ratio. To mitigate contamination of cortical GM intensity by intensities of WM and cerebrospinal fluid (CSF), the tissue fraction effect was corrected in individual T1w/T2w ratio maps using the geometric transfer matrix-derived region-based voxel-wise method implemented in *PETsurfer* [32]. Finally, individual T1w/T2w ratio maps were projected onto the average cortical surface of the sample, and smoothed using non-linear spherical wavelet-based denoising schemes [33]. All processing steps were visually checked for quality assurance.

Amyloid PET acquisition and preprocessing

To estimate global A β load in the brain, participants were injected with 300 MBq of ¹⁸F-Florbetaben (FBB, NeuraCeq™, Piramal Pharma) 90 min before image acquisition in a Philips Gemini 16 PET/CT scanner (Philips, Best, Netherlands). PET data were corrected for radioactive decay, dead time, attenuation, and scatter. Cerebral PET images were reconstructed iteratively with an isotropic voxel resolution of 2 mm³. Participants underwent a 20-min FBB-PET scan in dynamic mode consisting of four frames of 5 min each. Each frame was inspected for excessive motion. As no excessive head motion was detected in scanned images, the four frames were averaged to create a single static FBB brain image used for quantitative analysis.

Partial volume correction (PVC) of FBB PET images was performed with *PetSurfer*. For this, we employed the geometric transfer matrix-derived region-based voxel-wise method assuming a uniform 6 mm point spread function. Next, PVC-cortical FBB images were transformed into standardized uptake value ratio (SUVR) using the mean PVC uptake of the cerebellar GM as reference region. Finally, we obtained the global cortical

A β load for each participant using an FBB composite extracted across 4 large bilateral regions: frontal (orbitofrontal cortex/inferior frontal gyrus/middle frontal gyrus/superior frontal gyrus/frontal pole), cingulate (anterior cingulate/posterior cingulate/isthmus cingulate), parietal (precuneus/inferior parietal cortex/superior parietal cortex/supramarginal gyrus), and lateral temporal (middle temporal/superior temporal gyri) [34].

Functional MRI preprocessing and rs-FC analysis

The rs-fMRI data were preprocessed using AFNI functions (<https://afni.nimh.nih.gov/afni>), version AFNI_20.3.01. For each participant, high-frequency spikes were eliminated (*3dDespike*), time-locked cardiac (measured by pulse oximeter) and respiratory motion artifacts on brain BOLD signals were minimized using RETROICOR [35], time differences in slice-acquisition were corrected (*3dTshift*), EPI scans were aligned using rigid body motion correction and the first volume as reference (*3dVolreg*), and aligned EPI scans were co-registered to their corresponding T1w volumes (*align_epi_anat.py*; cost function: lpc+ZZ).

Dynamics were removed provided that more than 5% of voxels exhibited signal intensities that deviated from the median absolute deviation of time series (*3dOutcount*), and/or when the Euclidean norm (*enorm*) threshold exceeded 0.3 mm in head motion. None of the participants showed more than 20% of artifactual dynamics after applying censoring. Simultaneous regression was further applied to minimize the impact of non-neuronal fluctuations on the rs-fMRI signal (*3dTproject*). Nuisance regressors included: i) six head motion parameters (3 translational and 3 rotational) derived from the EPI scan alignment along with their first-order derivatives, ii) time series of mean total WM/CSF signal intensity, and iii) cardiac and respiratory fluctuations plus their derivatives to mitigate effects of extracerebral physiological artifacts on brain BOLD signals.

Preprocessed rs-fMRI scans were projected onto the 5th-order icosahedral tessellation of the average cortical surface. Seeds for rs-FC analyses were obtained from cortical regions showing significant correlations between global A β load and T1w/T2w ratio maps. Surface-based rs-FC seed to whole cortex maps were computed using the Fisher's z-transform of the corresponding Pearson's correlation coefficients.

Statistical analysis

We first performed vertex-wise multiple linear regression analyses to evaluate associations between global A β load and T1w/T2w ratio maps. These analyses were adjusted by age, sex, education years, body mass index (BMI), insulin resistance estimated with the homeostasis model assessment (HOMA-IR) [36], and metabolic status evaluated as a continuous score [37]. The clusters resulting from this analysis were used as seeds to generate the rs-FC maps aimed at evaluating whether significant and positive rs-FC patterns were moderated by the interaction between global A β load and mean T1w/T2w ratio of the region used as seed in the rs-FC map. These models were also adjusted by the above-mentioned covariates.

Vertex-wise regression analyses for cortical T1w/T2w ratio and rs-FC were performed with the SurfStat package (<https://www.math.mcgill.ca/keith/surfstat/>). Results were corrected for multiple comparisons using a hierarchical statistical model that first controls the family-wise error rate at the cluster level by applying random field theory over smoothed statistical maps ($p_{\text{vertex}} < 0.001$, $p_{\text{cluster}} < 0.05$), and next controls the false discovery rate at the vertex level within each cluster ($p < 0.05$) over unsmoothed statistical maps [38]. Peaks of clusters that survived correction for multiple comparisons were employed to establish the anatomical location of significant changes using the Desikan-Killiany atlas [39].

After inferential evidence of a main effect, the standardized measure of effect size (i.e., Cohen's f^2) was obtained to evaluate the local effect size for a multivariate regression model [40]. To establish the precision of standardized effect sizes, we computed 95% confidence intervals ($CI_{95\%}$) with the Matlab's *bootci* function using the normal approximated interval with bootstrapped bias and standard error ($N = 10,000$ bootstrap samples).

For each cortical vertex showing the maximum statistic within each significant cluster, we further applied Bayesian linear regression analyses using JASP, version 0.12.2 (<https://jasp-stats.org/>). The Bayesian approach allowed us to quantify the evidence for the alternative hypothesis and to overcome the problem of multiple comparisons across contrasts. Bayesian linear regression analyses were based on the Jeffreys-Zellner-Siow prior with an r scale of 0.354 [41]. The strength of the Bayes factor for the model including all covariates of no interest (null model) was compared with the model including the predictor of interest (experimental model) (BF_{10}). The

classification scheme proposed by Lee and Wagenmakers was employed to interpret the BF_{10} [42]. Clusters were reported as long as the p value yielded by the frequentist approach was < 0.05 , the standardized size effect was at least small, and the evidence in favor of the alternative hypothesis was at least moderate ($BF_{10} \geq 3$).

Next, we evaluated whether cortical regions showing a significant association of global A β load with either T1w/T2w ratio or rs-FC accounted for the variability in cognitive function. For this, we first applied the Yeo-Johnson transformation to the cognitive scores to mitigate the detrimental effects of skewedness and heteroscedasticity on different models [43]. We next built three models to assess the main and interaction effects. The first model (null model) only included the covariates of no interest, while the experimental models included either the mean T1w/T2w ratio or the mean rs-FC in a particular cluster as the main regressor of interest. The experimental and null models were compared with an ANOVA by applying both frequentist and Bayesian approaches.

Finally, we assessed whether associations between A β -related changes in T1w/T2w ratio and cognitive performance were mediated, at least partially, by global A β load. For this, we performed causal mediation analysis using the *mediate* function of the Mediation R package. Unstandardized indirect effects were computed for each of 1000 bootstrapped samples using 95% bias-corrected and accelerated confidence intervals at the 2.5th and 97.5th percentiles.

RESULTS

Relationship between global A β load and T1w/T2w ratio

We first identified those cortical regions where the T1w/T2w ratio varied with global A β load. The results of multiple regression analyses are displayed in Fig. 1 and summarized in Table 2. The direction of the relationship was negative in the left anterior cingulate, left lingual gyrus and different areas of the right inferior frontal gyrus, whereas it was positive in the left parahippocampal gyrus, right frontoparietal regions, and posterior cingulate bilaterally. Remarkably, the effect sizes were highest in the right posterior cingulate and left parahippocampal gyrus, two cortical regions showing positive correlations between global A β load and T1w/T2w ratio. Bayesian linear regression analyses showed extreme evidence for the positive associations in the right medial orbitofrontal and the posterior cingulate bilaterally (Table 2).

Effects of global A β load on the relationship between T1w/T2w ratio and rs-FC

We further assessed whether the strength of rs-FC shown by cortical regions exhibiting correlations between T1w/T2w ratio and global A β load differed as a function of global A β burden. Results of the frequentist and Bayesian approaches are summarized in Table 3. Multiple regression analyses revealed a moderating effect of global A β load for the association between T1w/T2w ratio in the right pars triangularis and the magnitude of rs-FC between this region and left superior frontal gyrus (Fig. 2, left upper panel). Post hoc analyses showed a negative association for participants showing global A β values 1 standard deviation (SD) above the mean while it was non-significant for those cases showing global A β values 1 SD below the mean (Fig. 2A, left bottom panel). A similar moderating effect was found for the association of T1w/T2w ratio in the left parahippocampal gyrus with rs-FC between this region and the left temporal pole (Fig. 2B, right upper panel). This significant association was negative for participants with higher global A β load and non-significant for the group with lower global A β load (Fig. 2B, right bottom panel).

Associations with cognition

We then investigated whether cognitive scores were associated with cortical regions affected by the relationship between global A β load and T1w/T2w ratio. The results of the frequentist and Bayesian approach are summarized in Table 4. Multiple regression analyses showed negative associations between general cognition (g factor), speed processing, attention and planning with T1w/T2w

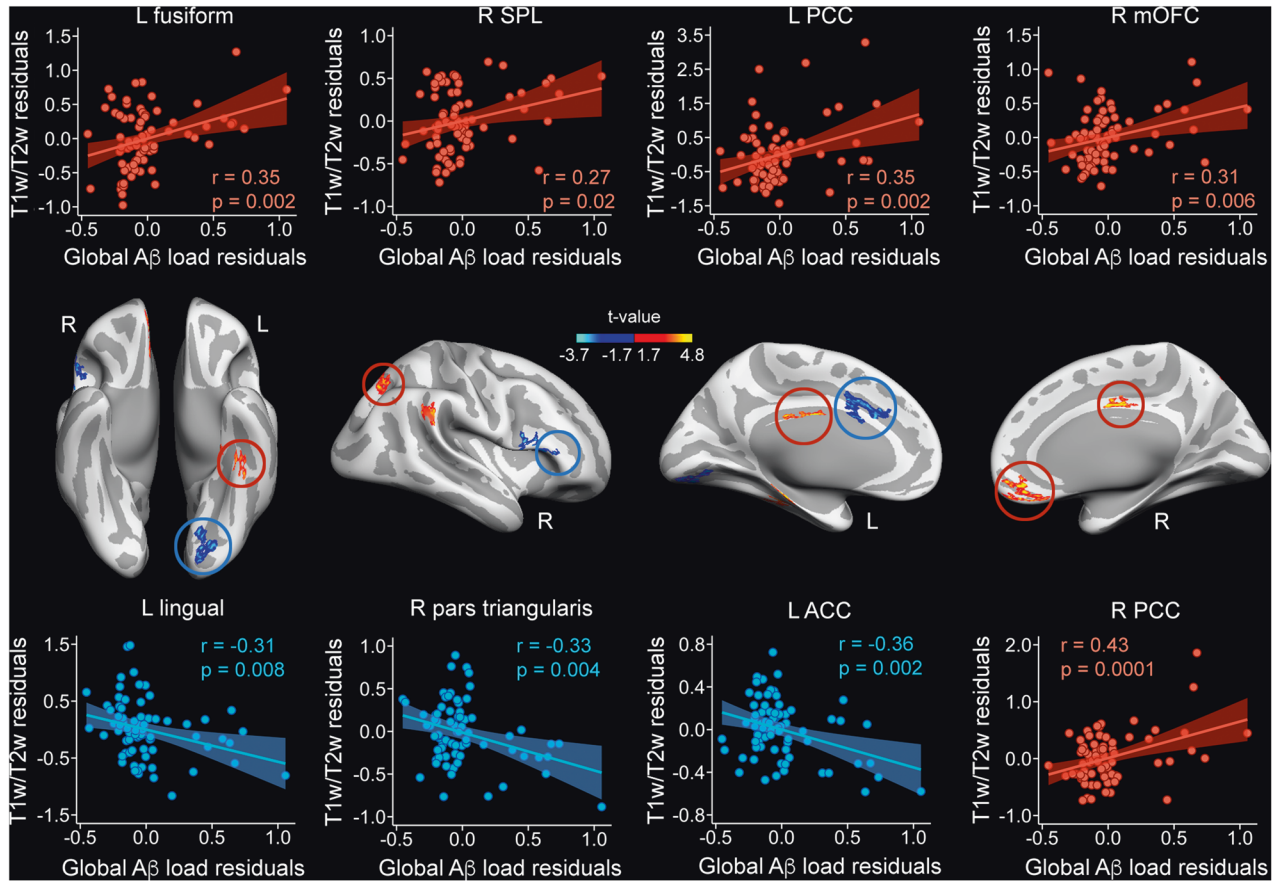


Fig. 1 Partial regression plots showing significant correlations between global A β load and T1w/T2w ratio. Scatter plots (upper and bottom panels) show positive (red) and negative (blue) correlations in cortical regions marked in red and blue circles, respectively (middle panel). Figure axes show the residuals from the T1w/T2w ratio and the rs-FC. SPL superior parietal lobe, PCC posterior cingulate cortex, mOFC medial orbitofrontal cortex, ACC anterior cingulate cortex. Right: right, L: left.

Table 2. Cortical regions showing significant correlations between global A β load and myelin content.

	MNI	R ²	F _{13,60}	f ² _{local}	CI _{95%}	BF ₁₀
<i>Negative correlations</i>						
L anterior cingulate ($p_{cluster} = 0.002$)	-11 18 32	0.13	10.8	0.14	0.008–0.49	26 ^S
L lingual gyrus ($p_{cluster} = 0.002$)	-25–80–9	0.15	12.8	0.10	0.01–0.28	6 ^M
R pars opercularis ($p_{cluster} = 0.008$)	46 10 20	0.16	13.4	0.11	0.004–0.36	6 ^M
R pars triangularis ($p_{cluster} = 0.02$)	52 23 11	0.15	12.9	0.12	0.02–0.45	67 ^{VS}
<i>Positive correlations</i>						
L posterior cingulate ($p_{cluster} = 0.01$)	-3–8 29	0.19	17.4	0.14	0.005–0.5	12355 ^E
L fusiform ($p_{cluster} = 0.02$)	-3–8 29	0.15	13	0.14	0.01–0.47	17 ^S
L parahippocampal ($p_{cluster} = 0.04$)	-22–21–18	0.25	23.4	0.22	0.008–0.74	31 ^{VS}
R medial orbitofrontal ($p_{cluster} = 0.00008$)	7 39–11	0.17	15.1	0.11	0.0002–0.41	12508 ^E
R superior parietal ($p_{cluster} = 0.001$)	4–62 7	0.13	10.5	0.10	0.0008–0.28	3.2 ^M
R supramarginal ($p_{cluster} = 0.01$)	65–37 30	0.14	12.1	0.14	0.02–0.41	63 ^{VS}
R posterior cingulate ($p_{cluster} = 0.02$)	6–8 42	0.20	18.2	0.22	0.02–0.73	100 ^E

MNI coordinates are in MNI152 space. f^2 : measure of local effect size. CI_{95%}: 95% confidence interval. BF₁₀: Bayes factor derived from Bayesian linear regression analyses. The superscript of the BF₁₀ indicates the qualitative interpretation of the evidence for the alternative hypothesis: ^M moderate; ^S strong; ^{VS} very strong; ^E extreme. L: left; R: right.

ratio in the posterior cingulate cortex (left or right hemisphere depending on the cognitive domain). Results further indicated a negative relationship between associative memory and T1w/T2w ratio in the left parahippocampal cortex. The largest effect sizes

were observed for the g factor in the left posterior cingulate followed by speed processing in the same region and by associative memory in the left parahippocampal gyrus. Bayesian linear regression analyses showed extreme evidence for the

negative correlations between the g factor and the posterior cingulate bilaterally (Table 4).

The mediating role of global A β load was only evident for the association between T1w/T2w ratio in the left posterior cingulate cortex and processing speed. More specifically, causal mediation analysis showed significant regression coefficients between the T1w/T2w ratio of the left posterior cingulate and global A β load ($0.15, p < 10^{-5}$) and between global A β load and processing speed ($3.86, p = 0.017$). The bootstrapped unstandardized indirect effect was 0.58, the 95% confidence interval ranged from 0.087 to 1.27, and the indirect effect was statistically significant ($p = 0.02$). However, the mediation was partial because the association between T1w/T2w ratio and processing speed remained different from zero when global A β load was introduced as a mediator.

Finally, we investigated whether the cognitive performance was also associated with patterns of rs-FC of cortical regions that previously showed a significant global A β load \times T1w/T2w ratio. The Bayesian approach only revealed an association of mental flexibility with rs-FC between right pars triangularis and left superior frontal gyrus ($BF_{10} = 3.84$), which, however, could not be confirmed by the frequentist approach ($F_{1,65} = 3.5, p = 0.06$).

DISCUSSION

Accumulation and deposition of A β in the brain, considered as the key initial step in AD pathogenesis, is inevitable with advancing age. Approximately 25% of cognitively normal older individuals show evidence of A β pathology [1, 44, 45]. Therefore, determining the initial effects of A β burden, before cognitive decline occurs,

Table 3. Effects of global A β load on the relationship between cortical myelin content and rs-FC.

FC seed Peak location of significant result	Extent of change (mm ²)	MNI coordinates	F	P	f^2
R pars triangularis					
L superior frontal gyrus	723	-10 20 35	14.4	10^{-2}	0.2_M
L parahippocampal					
L temporal pole	243	-39 8-36	12.3	10^{-2}	0.17_M

MNI coordinates correspond to MNI152 standard space. P: p value of the cluster; f^2 : measure of global effect size. Effect size (f^2): small (S) ≥ 0.02 , medium (M) ≥ 0.15 , large (L) ≥ 0.35 . L/R: left/right.

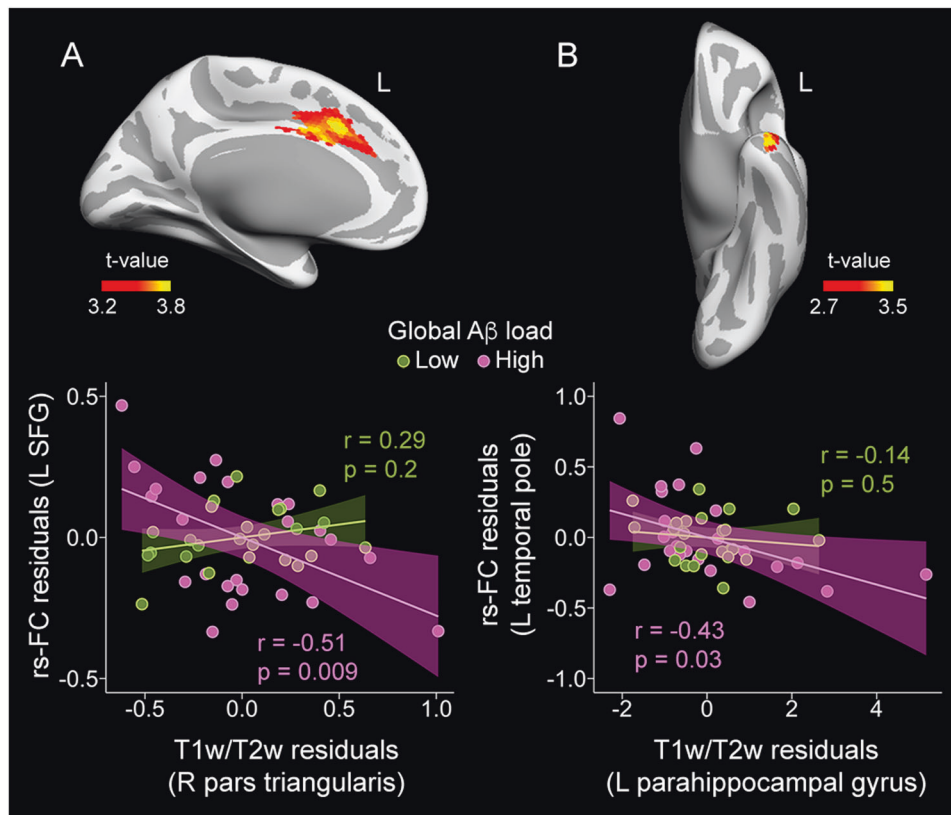


Fig. 2 Partial regression plots showing the moderating effect of A β -related intracortical myelin changes on rs-FC networks. **A** Pattern of rs-FC using the right pars triangularis as FC seed (upper panel). Participants showing values 1 SD above the mean of global A β load (pink) revealed significant negative associations between T1w/T2w ratio in the right pars triangularis and rs-FC in the left superior frontal gyrus (SFG). **B** Abnormal pattern of rs-FC using the left parahippocampal gyrus as FC seed (upper panel). Participants showing values 1 SD above the mean of global A β load (pink) revealed significant negative associations between T1w/T2w ratio in the left parahippocampal gyrus and rs-FC in the left temporal pole. Figure axes show the residuals from the T1w/T2w ratio and the rs-FC.

Table 4. Association of cognition with global A β load-induced changes in cortical myelin content.

	beta	F _{1,66}	p	Size effect	CI _{95%}	BF ₁₀
<i>g factor</i>						
L posterior cingulate	-0.78	27.9	10 ⁻⁵	0.24	0.02–0.72	180 ^E
R posterior cingulate	-1.42	6.7	0.01	0.09	0.002–0.40	171 ^E
<i>Associative memory</i>						
L parahippocampal	-1.78	6.3	0.01	0.13	0.01–0.37	8.8 ^M
<i>Processing speed</i>						
L posterior cingulate	-0.93	9.8	0.002	0.19	0.02–0.55	56 ^{VS}
R posterior cingulate	-2.25	4.2	0.04	0.09	0.001–0.57	3.7 ^M
<i>Attention</i>						
R posterior cingulate	-1.28	7.6	0.007	0.11	0.007–0.33	7.3 ^M
<i>Planning</i>						
L posterior cingulate	-0.46	5.5	0.02	0.08	0.001–0.30	3.3 ^M

CI_{95%}: 95% confidence interval. BF₁₀: Bayes factor derived from Bayesian linear regression analyses. The superscript of the BF₁₀ indicates the qualitative interpretation of the evidence for the alternative hypothesis: ^M moderate; ^S strong; ^{VS} very strong; ^E extreme. L: left; R: right.

may be crucial for early detection and treatment of AD. Regardless of whether A β burden precedes or results from myelin damage, evidence suggests that myelin breakdown is one of the earliest abnormalities contributing to synaptic dysfunctions before the onset of AD symptoms [46]. The present study contributes to strengthen this view. Here, we showed that increased global A β uptake was related to changes in cortical myelin content in cognitively normal older adults. Both decreases and increases in cortical myelination linked to A β pathology were further associated with altered patterns of rs-FC and subclinical cognitive deficits. Collectively, these findings provide an unprecedented opportunity for noninvasive evaluation of the association between A β burden and cortical myelin content in cognitively normal older adults.

The association between A β burden and intracortical myelin has been previously described in post-mortem AD brain tissue. These studies have shown that damage of cortical myelinated axons occurred concomitantly with the appearance of amyloid precursor protein (APP) and was accompanied by an increased expression of degraded myelin basic protein that co-localized with both myelin sheaths and A β plaques [47]. Our findings agree with previous research carried out in humans [48, 49] and transgenic mouse models of AD [11, 50, 51], indicating that initial A β deposition relates to changes in the microstructural integrity of cortical GM years before the hypothetical onset of clinical symptoms. It is important to emphasize that A β -PET retention has shown to be helpful for monitoring the progression of demyelination across the AD continuum [52] and multiple sclerosis [53], suggesting that A β -PET radiotracers bind WM myelin and therefore are able to indirectly relate to myelin content in vivo.

In line with our initial hypothesis, greater A β burden was found to be associated with lower myelin content in the left lingual gyrus, left anterior cingulate, and right aspects of the inferior frontal gyrus. These results are consistent with previous studies that highlight the vulnerability of these cortical regions to AD pathology and myelin damage. Accordingly, we have recently reported lower myelin content in the left lingual gyrus of asymptomatic older adults carrying the ϵ 4 allele of the APOE gene [54]. This region has also shown lower strength of rs-FC in patients with mild cognitive impairment [55] and decreased activation while AD patients performed a memory task [56]. Similarly, higher A β retention in the anterior cingulate cortex has been associated with the development of preclinical AD [57]. Furthermore, recent research has revealed that greater global A β deposition is associated with higher activation of the right inferior

frontal gyrus in cognitively normal older adults [58], supporting abnormal activation of this region in preclinical AD [59]. All these late-myelinating cortical regions are particularly susceptible to early AD pathology and, consequently, more prone to experience myelin breakdown [60]. Alternatively, A β pathology may result from the age-related increase in the need for myelin maintenance and repair, suggesting that A β burden is secondary to brain efforts to maintain myelin homeostasis [61].

Previous research has demonstrated that cerebral A β burden is also accompanied by an increase in oligodendrogenesis paralleled by thicker myelin sheaths and shorter nodes of Ranvier in transgenic mouse models of AD [13, 14]. These results are consistent with our data showing positive correlations between global A β load and cortical myelin content. Other studies have also shown abnormally higher myelination patterns in cortical regions that accumulate A β deposition before the onset of AD symptoms [62, 63]. These findings are interpreted as a compensatory remyelination in affected cortical regions [64], which may alter the speed of axonal conduction caused by shorter internodes of remyelinated axons [20, 65]. In line with this hypothesis, we found that global A β load partially mediated the negative association between myelin content in the left posterior cingulate gyrus and processing speed. These results support the idea that signaling pathways involved in both A β accumulation and myelin repair could contribute to deterioration in cognitive functioning [66].

Subtle changes in myelin thickness and/or internodal structure have profound effects on neuronal network function affecting spike-time arrival [20], which is of fundamental importance for neural coding, neuronal integration and synaptic plasticity [21]. Similarly, the frequency, propagation and coupling of intrinsic oscillatory neuronal activity within cortical networks is also strongly influenced by conduction delays and thus by myelin integrity of small-caliber cortical axons [67]. Consequently, conduction delays in myelinated cortical axons originated by external insults may ultimately lead to abnormal synchronization patterns of cortical networks. Consistent with these findings, older individuals with greater A β burden showed abnormal patterns of rs-FC of the pars triangularis and parahippocampal gyrus. However, abnormal patterns of rs-FC were not correlated with cognition, leading us to speculate that the negative impact of such functional reorganization may become evident when the cognitive decline begins and/or in presence of tau pathology.

Multiple lines of evidence support that altered myelination may be one of the mechanisms by which amyloid pathology leads to

cognitive decline. First, A β deposits, which initially tend to spread into the neocortex², may alter functional communication not only by disrupting intracellular calcium homeostasis and synaptic transmission in cortical networks [68, 69], but also by damaging myelinated cortical neurons, which are supposed to play a major role in synchronizing conduction velocity within cortical circuits [70]. Second, damage of myelinated cortical axons may also increase the metabolic requirements of cortical neurons to maintain neurotransmission levels [71]. This high-energy expenditure increases the production of free radicals, making oligodendrocytes especially vulnerable to oxidative insults [72]. This hypothesis is consistent with recent findings suggesting that oligodendrocytes are part of a neuronal antioxidant defense system to support iron detoxification [73]. Third, oligodendrocytes are not only responsible for axonal myelination but also for the synthesis of brain cholesterol [74]. About 70% of the cholesterol in the brain resides in axonal myelin sheaths, enabling the current to move down the axon rather than diffusing across the membrane [75]. The fact that aggregated A β shows high affinity for cholesterol binding in the cell membrane [76] could also lead to myelin damage and enhanced A β -induced toxicity in cortical networks [77]. The association between A β deposition and myelin breakdown could be bidirectional. Indeed, recent evidence has shown that myelin damage induced in mouse models of amyloidosis are also capable of driving A β deposition by shifting neuronal APP metabolism and by altering the microglial phenotype [17]. On the basis of these findings, we speculate that aging-dependent myelin loss may contribute to the appearance of initial A β deposits, whereas at later stages, A β aggregates may facilitate the downstream effects of A β and tau pathology in oligodendrocytes and their precursor cells.

This study has several limitations. First, changes in cortical T1w/T2w ratio maps could be influenced by factors other than demyelination [78, 79]. Accordingly, these results should be interpreted cautiously until the biological interpretation of cortical T1w/T2w ratio maps is more precise. On the other hand, these results are derived from a cross-sectional study. Therefore, they cannot shed light into how the relationship between global A β load and cortical myelination affects AD development or into the causal effects of A β burden on intracortical myelin and/or vice versa. Furthermore, the degree of AD pathology was only established for A β pathology. Further studies should assess if cortical myelin content is also related to the presence of abnormal tau biomarkers in cognitively normal older adults. Finally, our results were obtained with a small sample and therefore they should be considered as preliminary and replicated in further experiments with a larger and independent cohort.

In conclusion, we have shown that the global A β burden is related to changes in the cortical microstructure from very early on, likely affecting myelinated axons of cortical GM, as revealed by changes in cortical T1w/T2w ratio maps. Myelin alterations associated with A β pathology were further related to abnormal patterns of rs-FC and subclinical cognitive deficits. Although we are still far from understanding the role of myelin damage in aging and preclinical AD, these results reinforce the view that A β aggregates and intracortical myelin are coupled events that may accelerate cognitive decline, ultimately increasing the risk to develop AD.

DATA AVAILABILITY

The datasets generated during the current study are available from the corresponding author on reasonable request.

REFERENCES

- Aizenstein HJ, Nebes RD, Saxton JA, Price JC, Mathis CA, Tsopelas ND, et al. Frequent amyloid deposition without significant cognitive impairment among the elderly. *Arch Neurol*. 2018;65:1509–17.

- Braak H, Braak E. Frequency of stages of Alzheimer-related lesions in different age categories. *Neurobiol Aging*. 1997;18:351–7.
- Jack CR Jr, Holtzman DM. Biomarker modeling of Alzheimer's disease. *Neuron* 2013;80:1347–58.
- Price JL, Morris JC. Tangles and plaques in nondemented aging and "preclinical" Alzheimer's disease. *Ann Neurol*. 1999;45:358–68.
- Sojkova J, Zhou Y, An Y, Kraut MA, Ferrucci L, Wong DF, et al. Longitudinal patterns of β -amyloid deposition in nondemented older adults. *Arch Neurol* 2011;68:644–9.
- Musiek ES, Holtzman DM. Three dimensions of the amyloid hypothesis: time, space and 'wingmen'. *Nat Neurosci*. 2015;18:800–6.
- Landau SM, Horng A, Jagust WJ. Alzheimer's Disease Neuroimaging Initiative. Memory decline accompanies subthreshold amyloid accumulation. *Neurology* 2013;90:e1452–60.
- Xu J, Chen S, Ahmed SH, Chen H, Ku G, Goldberg MP, et al. Amyloid-beta peptides are cytotoxic to oligodendrocytes. *J Neurosci*. 2001;21:RC118.
- Lee JT, Xu J, Lee JM, Ku G, Han X, Yang DI, et al. Amyloid-beta peptide induces oligodendrocyte death by activating the neutral sphingomyelinase-ceramide pathway. *J Cell Biol*. 2004;164:123–31.
- Horiuchi M, Maezawa I, Itoh A, Wakayama K, Jin LW, Itoh T, et al. Amyloid β 1-42 oligomer inhibits myelin sheet formation in vitro. *Neurobiol Aging*. 2012;33:499–509.
- Desai MK, Mastrangelo MA, Ryan DA, Sudol KL, Narrow WC, Bowers WJ. Early oligodendrocyte/myelin pathology in Alzheimer's disease mice constitutes a novel therapeutic target. *Am J Pathol*. 2010;177:1422–35.
- Behrendt G, Baer K, Buffo A, Curtis MA, Faull RL, Rees MI, et al. Dynamic changes in myelin aberrations and oligodendrocyte generation in chronic amyloidosis in mice and men. *Glia* 2013;61:273–86.
- Wu Y, Ma Y, Liu Z, Geng Q, Chen Z, Zhang Y. Alterations of myelin morphology and oligodendrocyte development in early stage of Alzheimer's disease mouse model. *Neurosci Lett*. 2017;642:102–6.
- Ferreira S, Pitman KA, Wang S, Summers BS, Bye N, Young KM, et al. Amyloidosis is associated with thicker myelin and increased oligodendrogenesis in the adult mouse brain. *J Neurosci Res*. 2020;98:1905–32.
- Stokin GB, Lillo C, Falzone TL, Brusch RG, Rockenstein E, Mount SL, et al. Axonopathy and transport deficits early in the pathogenesis of Alzheimer's disease. *Science* 2005;307:1282–88.
- Desai MK, Sudol KL, Janelins MC, Mastrangelo MA, Frazer ME, Bowers WJ. Triple-transgenic Alzheimer's disease mice exhibit region-specific abnormalities in brain myelination patterns prior to appearance of amyloid and tau pathology. *Glia* 2009;57:54–65.
- Depp C, Nave KA. Ageing-associated myelin dysfunction drives amyloid deposition in mouse models of Alzheimer's disease. *Alzheimer's Dement*. 2022;18:e061183.
- Pareto D, Garcia-Vidal A, Alberich M, Auger C, Montalban X, Tintoré M, et al. Ratio of T1-weighted to T2-weighted signal intensity as a measure of tissue integrity: comparison with magnetization transfer ratio in patients with multiple sclerosis. *AJNR Am J Neuroradiol*. 2020;41:461–3.
- Glasser MF, Van Essen DC. Mapping human cortical areas in vivo based on myelin content as revealed by T1- and T2-weighted MRI. *J Neurosci*. 2011;31:11597–616.
- Pajevic S, Basser PJ, Fields RD. Role of myelin plasticity in oscillations and synchrony of neuronal activity. *Neurosci*. 2014;276:135–47.
- Fields RD. A new mechanism of nervous system plasticity: activity-dependent myelination. *Nat Rev Neurosci*. 2015;16:756–67.
- Monje M. Myelin plasticity and nervous system function. *Annu Rev Neurosci*. 2018;41:61–76.
- Noori R, Park D, Griffiths JD, Bells S, Frankland PW, Mabbott D, et al. Activity-dependent myelination: A glial mechanism of oscillatory self-organization in large-scale brain networks. *Proc Natl Acad Sci USA*. 2020;117:13227–37.
- Lu PH, Lee GJ, Tishler TA, Meghpara M, Thompson PM, Bartzokis G. Myelin breakdown mediates age-related slowing in cognitive processing speed in healthy elderly men. *Brain Cogn*. 2013;81:131–8.
- Gong Z, Bilgel M, Kiely M, Triebswetter C, Ferrucci L, Resnick SM, et al. Lower myelin content is associated with more rapid cognitive decline among cognitively unimpaired individuals. *Alzheimers Dement*. (in press). <https://doi.org/10.1002/alz.12968>.
- Böhm P, Peña-Casanova J, Aguilar M, Hernández G, Sol JM, Blesa R. Clinical validity and utility of the interview for deterioration of daily living in dementia for Spanish-speaking communities NORMACODEM Group. *Int Psychogeriatr*. 1998;10:261–70.
- Sheikh JL, Yesavage JA. Geriatric Depression Scale (GDS): Recent evidence and development of a shorter version. *Clin Gerontol*. 1986;5:165–73.
- Gramunt N, Sánchez-Benavides G, Buschke H, Diéguez-Vide F, Peña-Casanova J, Masramon X, et al. The memory binding test: Development of two alternate forms into Spanish and Catalan. *J Alzheimers Dis*. 2016;52:283–93.

29. Alegret M, Valero S, Ortega G, Espinosa A, Sanabria A, Hernández I, et al. Validation of the Spanish version of the Face Name Associative Memory Exam (S-FNAME) in cognitively normal older individuals. *Arch Clin Neuropsychol*. 2015;30:712–20.
30. Fischl B, Dale AM. Measuring the thickness of the human cerebral cortex from magnetic resonance images. *Proc Natl Acad Sci USA*. 2001;97:11050–5.
31. Greve DN, Fischl B. Accurate and robust brain image alignment using boundary-based registration. *Neuroimage* 2009;48:63–72.
32. Greve DN, Salat DH, Bowen SL, Izquierdo-Garcia D, Schultz AP, Catana C, et al. Different partial volume correction methods lead to different conclusions: An (18) F-FDG-PET study of aging. *Neuroimage* 2016;132:334–43.
33. Bernal-Rusiel JL, Atienza M, Cantero JL. Detection of focal changes in human cortical thickness: spherical wavelets versus Gaussian smoothing. *Neuroimage* 2008;41:1278–92.
34. Mormino EC, Betensky RA, Hedden T, Schultz AP, Ward A, Huijbers W, et al. Amyloid and APOE E4 interact to influence short-term decline in preclinical Alzheimer disease. *Neurology*. 2014;82:1760–7.
35. Glover GH, Li TQ, Ress D. Image-based method for retrospective correction of physiological motion effects in fMRI: RETROICOR. *Magn Reson Med*. 2000;44:162–7.
36. Matthews DR, Hosker JP, Rudenski AS, Naylor BA, Treacher DF, Turner RC. Homeostasis model assessment: insulin resistance and beta-cell function from fasting plasma glucose and insulin concentrations in man. *Diabetologia* 1985;28:412–9.
37. Soldatovic I, Vukovic R, Culafic D, Gajic M, Dimitrijevic-Sreckovic V. siMS score: simple method for quantifying metabolic syndrome. *PLoS One*. 2016;11:e0146143.
38. Bernal-Rusiel JL, Atienza M, Cantero JL. Determining the optimal level of smoothing in cortical thickness analysis: a hierarchical approach based on sequential statistical thresholding. *Neuroimage* 2010;52:158–71.
39. Desikan RS, Ségonne F, Fischl B, Quinn BT, Dickerson BC, Blacker D, et al. An automated labeling system for subdividing the human cerebral cortex on MRI scans into gyral based regions of interest. *Neuroimage* 2006;31:968–80.
40. Cohen JE. (ed). *Statistical power analysis for the behavioral sciences*. 1988. Hillsdale, NJ: Lawrence Erlbaum Associates.
41. Liang F, Paulo R, Molina G, Clyde MA, Berger JO. Mixtures of g priors for Bayesian variable selection. *J Am Stat Assoc*. 2008;103:410–23.
42. Lee MD, Wagenmakers EJ (eds). *Bayesian cognitive modeling: A practical course* 2013. Cambridge University Press.
43. Yeo IK, Johnson RA. A new family of power transformations to improve normality or symmetry. *Biometrika* 2000;87:954–9.
44. Jack CR Jr, Wiste HJ, Weigand SD, Rocca WA, Knopman DS, Mielke MM, et al. Age-specific population frequencies of cerebral β -amyloidosis and neurodegeneration among people with normal cognitive function aged 50–89 years: a cross-sectional study. *Lancet Neurol*. 2014;13:997–1005.
45. Jansen WJ, Ossenkoppele R, Knol DL, Tijms BM, Scheltens P, Verhey FR, et al. Prevalence of cerebral amyloid pathology in persons without dementia: a meta-analysis. *J Am Med Assoc*. 2015;313:1924–38.
46. Papuč E, Rejdak K. The role of myelin damage in Alzheimer's disease pathology. *Arch Med Sci*. 2018;16:345–51.
47. Zhan X, Jickling GC, Ander BP, Stamova B, Liu D, Kao PF, et al. Myelin basic protein associates with A β PP, A β 1–42, and amyloid plaques in cortex of Alzheimer's disease brain. *J Alzheimers Dis*. 2015;44:1213–29.
48. Dean DC 3rd, Hurley SA, Keckskemeti SR, O'Grady JP, Canda C, Davenport-Sis NJ, et al. Association of amyloid pathology with myelin alteration in preclinical Alzheimer disease. *JAMA Neurol*. 2017;74:41–9.
49. Luo X, Li K, Zeng Q, Huang P, Jiaerken Y, Wang S, et al. Application of T1-/T2-weighted ratio mapping to elucidate intracortical demyelination process in the Alzheimer's disease continuum. *Front Neurosci*. 2019;13:904.
50. Mitew S, Kirkcaldie MT, Halliday GM, Shepherd CE, Vickers JC, Dickson TC. Focal demyelination in Alzheimer's disease and transgenic mouse models. *Acta Neuropathol*. 2010;119:567–77.
51. Schmuied LC, Raymick J, Paule MG, Dumas M, Sarkar S. Characterization of myelin pathology in the hippocampal complex of a transgenic mouse model of Alzheimer's disease. *Curr Alzheimer Res*. 2013;10:30–7.
52. Moscoso A, Silva-Rodríguez J, Aldrey JM, Cortés J, Pías-Peleiteiro JM, Ruibal Á, et al. ¹⁸F-florbetapir PET as a marker of myelin integrity across the Alzheimer's disease spectrum. *Eur J Nucl Med Mol Imaging*. 2022;49:1242–53.
53. Pietroboni AM, Carandini T, Colombi A, Mercurio M, Ghezzi L, Giulietti G, et al. Amyloid PET as a marker of normal-appearing white matter early damage in multiple sclerosis: correlation with CSF β -amyloid levels and brain volumes. *Eur J Nucl Med Mol Imaging*. 2019;46:280–7.
54. Fernandez-Alvarez M, Atienza M, Canter JL. Effects of non-modifiable risk factors of Alzheimer's disease on intracortical myelin content. *Alzheimers Res Ther*. 2022;14:202.
55. Yuan B, Xie C, Shu H, Liao W, Wang Z, Liu D, et al. Differential effects of APOE genotypes on the anterior and posterior subnetworks of default mode network in amnesic mild cognitive impairment. *J Alzheimers Dis*. 2016;54:1409–23.
56. Scarmeas N, Anderson KE, Hilton J, Park A, Habeck C, Flynn J, et al. APOE-dependent PET patterns of brain activation in Alzheimer disease. *Neurology* 2004;63:913–5.
57. Brier MR, McCarthy JE, Benzinger TLS, Stern A, Su Y, Friedrichsen KA, et al. Local and distributed PiB accumulation associated with development of preclinical Alzheimer's disease. *Neurobiol Aging*. 2016;38:104–11.
58. Karim HT, Tudorascu DL, Cohen A, Price JC, Lopresti B, Mathis C, et al. Relationships between executive control circuit activity, amyloid burden, and education in cognitively healthy older adults. *Am J Geriatr Psychiatry*. 2019;27:1360–71.
59. Zeng Q, Luo X, Li K, Wang S, Zhang R, Hong H, et al. Distinct spontaneous brain activity patterns in different biologically-Defined Alzheimer's disease cognitive stage: a preliminary study. *Front Aging Neurosci*. 2019;11:350.
60. Braak H, Braak E. Development of Alzheimer-related neurofibrillary changes in the neocortex inversely recapitulates cortical myelogenesis. *Acta Neuropathol*. 1996;92:197–201.
61. Bartzokis G. Alzheimer's disease as homeostatic responses to age-related myelin breakdown. *Neurobiol Aging*. 2011;32:1341–71.
62. Yasuno F, Kazui H, Morita N, Kajimoto K, Ihara M, Taguchi A, et al. Use of T1-weighted/T2-weighted magnetic resonance ratio to elucidate changes due to amyloid β accumulation in cognitively normal subjects. *Neuroimage: Clin*. 2017;13:209–14.
63. Pelkmans W, Dicks E, Barkhof F, Vrenken H, Scheltens P, van der Flier WM, et al. Gray matter T1-w/T2-w ratios are higher in Alzheimer's disease. *Hum Brain Mapp*. 2019;40:3900–9.
64. Kwicien JM. Cellular compensatory mechanisms in the CNS of dysmyelinated rats. *Comp Med*. 2010;60:205–17.
65. Scurfield A, Latimer DC. A computational study of the impact of inhomogeneous internodal lengths on conduction velocity in myelinated neurons. *PLoS One*. 2018;13:e0191106.
66. Hirschfeld LR, Risacher SL, Nho K, Saykin AJ. Myelin repair in Alzheimer's disease: a review of biological pathways and potential therapeutics. *Transl Neurodegener*. 2022;11:47.
67. Nunez PL, Srinivasan R, Fields RD. EEG functional connectivity, axon delays and white matter disease. *Clin Neurophysiol*. 2015;126:110–20.
68. Mattson MP, Cheng B, Davis D, Bryant K, Lieberburg I, Rydel RE. β -Amyloid peptides destabilize calcium homeostasis and render human cortical neurons vulnerable to excitotoxicity. *J Neurosci*. 1992;12:376–89.
69. Kamenetz F, Tomita T, Hsieh H, Seabrook G, Borchelt D, Iwatsubo T, et al. APP processing and synaptic function. *Neuron* 2003;37:925–37.
70. Timmler S, Simons M. Grey matter myelination. *Glia* 2019;67:2063–70.
71. Hildebrand C, Remahl S, Persson H, Bjartmar C. Myelinated nerve fibres in the CNS. *Prog Neurobiol*. 1993;40:319–84.
72. Nave KA. Myelination and support of axonal integrity by glia. *Nature* 2010;468:244–52.
73. Mukherjee C, Kling T, Russo B, Miebach K, Kess E, Schifferer M, et al. Oligodendrocytes provide antioxidant defense function for neurons by secreting ferritin heavy chain. *Cell Metab*. 2020;32:259–72.
74. Björkhem I, Meaney S. Brain cholesterol: long secret life behind a barrier. *Arterioscler Thromb Vasc Biol*. 2004;24:806–15.
75. Snipes G, Suter U. Cholesterol and Myelin. In: Bittman R (ed). *Cholesterol*. New York: Plenum Press, 1998.
76. Avdulov NA, Chochina SV, Igbavboa U, Warden CS, Vassiliev AV, Wood WG. Lipid binding to amyloid beta-peptide aggregates: preferential binding of cholesterol as compared with phosphatidylcholine and fatty acids. *J Neurochem*. 1997;69:1746–52.
77. Rudajev V, Novotny J. Cholesterol as a key player in amyloid β -mediated toxicity in Alzheimer's disease. *Front Mol Neurosci*. 2022;15:937056.
78. Preziosa P, Bouman PM, Kiljan S, Steenwijk MD, Meani A, Pouwels PJ, et al. Neurite density explains cortical T1-weighted/T2-weighted ratio in multiple sclerosis. *J Neurol Neurosurg Psychiatry*. 2021;92:790–2.
79. Zheng Y, Dudman J, Chen JT, Mahajan KR, Herman D, Fox RJ, et al. Sensitivity of T1/T2-weighted ratio in detection of cortical demyelination is similar to magnetization transfer ratio using post-mortem MRI. *Mult Scler*. 2022;28:198–205.

ACKNOWLEDGEMENTS

This work was supported by the Spanish Ministry of Economy and Competitiveness (PID2020-119978RB-I00 to JLC, PID2020-118825GB-I00 to MA), CIBERNED (JLC), Alzheimer's Association (AARG-NTF-22-924702 to JLC), the Junta de Andalucía (PY20_00858 to JLC), and the Andalucía-FEDER Program (UPO-1380913 to JLC).

AUTHOR CONTRIBUTIONS

JLC conceived the study and wrote the first draft. MFA, JLC, and MA contributed to data acquisition, analysis, and preparation of tables and figures. All authors contributed to data interpretation and discussion of results, revised the article for important intellectual content, and approved the final version of the manuscript.

CONFLICT OF INTEREST

The authors declare no competing interests.

ADDITIONAL INFORMATION

Correspondence and requests for materials should be addressed to Jose L. Cantero.

Reprints and permission information is available at <http://www.nature.com/reprints>

Publisher's note Springer Nature remains neutral with regard to jurisdictional claims in published maps and institutional affiliations.



Open Access This article is licensed under a Creative Commons Attribution 4.0 International License, which permits use, sharing, adaptation, distribution and reproduction in any medium or format, as long as you give appropriate credit to the original author(s) and the source, provide a link to the Creative Commons license, and indicate if changes were made. The images or other third party material in this article are included in the article's Creative Commons license, unless indicated otherwise in a credit line to the material. If material is not included in the article's Creative Commons license and your intended use is not permitted by statutory regulation or exceeds the permitted use, you will need to obtain permission directly from the copyright holder. To view a copy of this license, visit <http://creativecommons.org/licenses/by/4.0/>.

© The Author(s) 2023